Supplementary Information

Supplementary Note 1: Sequence Design Principles and Complete Sequences

Design Overview

The CRISPR-condensate system required careful engineering at multiple levels: the guide RNA scaffold, the multivalent nanostar topology, the kissing-loop (KL) interaction interfaces, and the RNA aptamer core. Each component was designed with specific functional constraints in mind.

sgRNA scaffold engineering. We used the Standard F+ sgRNA scaffold (76 nt) variant as the backbone for all chimeric designs. This scaffold contains two additional stem loops (the 3' hairpin and the nexus loop) relative to the minimal F+ configuration, providing additional transcriptional handle sites and improving overall structural stability. The F+E scaffold was chosen based on prior observations that extended scaffolds support stronger dCas9 binding and enhanced transcriptional effector recruitment at target loci. The nanostar fusion point was positioned downstream of the terminal nexus loop to minimize steric interference with dCas9 ribonucleoprotein assembly. NUPACK predictions confirm that the sgRNA scaffold (nucleotides 1-85) maintains its native secondary structure (pairing probability >0.95 for all stem regions) independently of the nanostar domain folding.

Nanostar arm design. Each nanostar arm contains a terminal 9-nucleotide KL motif, comprising a 6-nucleotide interaction sequence flanked by three unpaired adenines, followed by a 6-nucleotide flexible linker and a 15- or 20-nucleotide stem which hybridizes with the complementary arm of a neighbouring monomer. The 6-nt linker is thought to confer rotational freedom between the KL recognition motif and the ds stem, enabling the multivalent assembled core to reach a more compact conformation. The stem sequences were selected to have melting temperatures of 55-60 degC to ensure stable arm pairing under physiological conditions while permitting thermal annealing during in vitro assembly.

Kissing-loop sequences. We examined four KL versions covering a spectrum of binding affinities: KL-A (5'-UCGCGA-3', predicted KD ~10 nM), KL-WT (5'-GCGCGC-3', predicted KD ~100 nM), KL-B (5'-GUCGAC-3', predicted KD ~1 uM), and KL-C (5'-GGUACC- 3', predicted KD ~10 uM). The KL-A sequence is derived from the DIS (dimerization initiation site) loop of HIV-1 genomic RNA and represents the strongest homodimerizing KL motif in this series. KL-WT is a variant with intermediate affinity. KL-B and KL-C provide progressively weaker interactions, allowing tunable condensate stability. All KL sequences were predicted with NUPACK (version 4.0.4) using the standard RNA energy model at 37 degC to confirm hairpin stability and dimerization propensity.

Aptamer cores. Three fluorescent aptamers were incorporated into nanostar designs: Broccoli (bound by DFHBI-1T), Pepper (bound by HBC530), and Mango (bound by TO1-biotin). Broccoli and Pepper were used for dual-color orthogonal imaging, while Mango provided a third channel for triple-labeling experiments. The MS2 coat protein-binding RNA stem-loop was incorporated into both activation- and repression-focused designs to recruit MCP-fused transcriptional effectors. Aptamer RNA secondary structures were evaluated in silico using NUPACK. Small-molecule ligand binding was not explicitly modeled.

NUPACK workflow. All RNA sequences were designed using an iterative NUPACK pipeline: (1) sequence specification of constraints (KL motifs, aptamer cores, stem regions), (2) sequence generation with pseudo-energy weighting for target secondary structures, (3) defect analysis to quantify the fraction of nucleotides incorrectly paired at equilibrium, (4) ensemble free energy validation to ensure the target structure dominates the Boltzmann distribution, and (5) dimerization and multimerization screening to rule out off-target aggregation. Designs with ensemble defect values below 5% were accepted for experimental testing.

Expression System

All nanostar sequences were expressed using the Tornado self-cleaving ribozyme system for RtcB-mediated RNA processing and circularization. The expression cassette contains: - U6+27 Pol III promoter - 5' twister ribozyme (teal) – generates 2',3'-cyclic phosphate - Nanostar sequence of interest (green) - 3' twister ribozyme (cyan) – generates 5'-hydroxyl - Endogenous RtcB ligase circularizes the processed RNA

The expression vector was pAV-U6+27-Tornado-Broccoli (Addgene #124360). Nanostar sequences were inserted between NotI-HF and SacII restriction sites via phosphorylated double-stranded oligonucleotides (IDT) or Gibson assembly.

Kissing Loop (KL) Sequences

All kissing loops are 9 nucleotides long, comprising a 6-nt palindromic interaction sequence flanked by 2 upstream and 1 downstream unpaired adenine (5'-AA…A-3').

KL Variant	Sequence (5'-3')	Estimated K_D	Source
KL-A	5'-AAUCGCGAA-3'	~10 nM	Fabrini et al. / Stewart 2024
KL-WT	5'-AAGCGCGCA-3'	~100 nM	HIV-1 palindromic KL
KL-B	5'-AAGUCGACA-3'	~1 uM	Fabrini et al.
KL-C	5'-AAGGUACCA-3'	~10 uM	Fabrini et al.
KL-E	5'-AAGUAUACA-3'	Intermediate	Designed (AU replacement)
KL-F	5'-AAAUAUAUA-3'	Weak	Designed (AU replacement)

sgRNA Scaffold Sequence (F+E Extended)

The sgRNA scaffold used in all chimeric designs is the Standard F+ variant:

> **F+E sgRNA scaffold:**
> GTTTTAGAGCTAGAAATAGCAAGTTAAAATAAGGCTAGTCCGTTATCAACTTG
> AAAAAGTGGCACCGAGTCGGTGC

This scaffold contains two additional stem loops (3' hairpin and nexus loop) relative to the minimal F+ configuration, providing enhanced dCas9 binding affinity. NUPACK predictions confirm that the scaffold maintains its native secondary structure (pairing probability >0.95 for all stem regions) independently of the nanostar domain folding.

Complete Nanostar-Module RNA Sequences

The sequences listed below correspond to the nanostar modules and do not include the upstream spacer or F+E sgRNA scaffold unless otherwise indicated. The following sequences represent the circularized nanostar products (Tornado-processed). Domain annotations: **arm** = stem-loop arm with KL; **Bro/Pep/Man** = fluorescent aptamer; **MS2** = MS2 coat protein-binding aptamer.

Primary Activation Constructs

15nt-KL A-Broccoli (15nt-3A-Br): > 5'-
GCGAGAGCGCUGCCCAAUCGCGAAGGGCAGCGCUCUCGCAAGGAUGGACGGUCGGGUCC
GAGGGCAAUCGCGAAGCCCUCGUCGAGUAGAGUGUGGGCCAUCCAAGCGUUCACACUGA
CCAAUCGCGAAGGUCAGUGUGAACGC-3'

- arm1 (Broccoli): GCGAGAGCGCUGCCCAAUCGCGAAGGGCAGCGCUCUCGC (29 nt, Broccoli aptamer underlined)
- arm2: GGAUGGACGGUCGGGUCCGAGGGCAAUCGCGAAGCCCUCGUCGAGUAGAGUGUG GGCCAUC (55 nt)
- arm3: GCGUUCACACUGACCAAUCGCGAAGGUCAGUGUGAACGC (33 nt)
- KL sites: AAUCGCGAA (x3)

15nt-KL WT-Broccoli: > 5'-
GCGAGAGCGCUGCCCAAGCGCGCAGGGCAGCGCUCUCGCAAGGAUGGACGGUCGGGUCC
GAGGGCAAGCGCGCAGCCCUCGUCGAGUAGAGUGUGGGCCAUCCAAGCGUUCACACUGA
CCAAGCGCGCAGGUCAGUGUGAACGC-3'

15nt-KL A-Pepper: > 5'-
GCGAGAGCGCUGCCCAAUCGCGAAGGGCAGCGCUCUCGCAACCGGGACCAAUCGUGGCG
UGUCGGCAGGGCAAUCGCGAAGCCCUGCACUGGCGCCGUCCCGGAAGCGUUCACACUGA
CCAAUCGCGAAGGUCAGUGUGAACGC-3'

15nt-KL A-Mango: > 5'-
GCGAGAGCGCUGCCCAAUCGCGAAGGGCAGCGCUCUCGCAAGCGAUGAACGUAGGGAAU

CGCGAACCCUACGUUCAUCGCAAGCGUUCACACUGACCAAUCGCGAAGGUCAGUGUGAA
CGCAAGGCACGUACGAAGGAGAGGAGAGGAAGAGGAGAGUACGUGCC-3’

20nt-KL A-Broccoli: > 5’-
GCGACGUGUUACGGCGAGGCAAUCGCGAAGCCUCGCCGUAACACGUCGCAAGGGCGAGG
ACGGUCGGGUCCGAGCGGUCAAUCGCGAAGACCGCUCGUCGAGUAGAGUGUGGGCCUCG
CCCAAGCUCCGCUCCCAGUGGGCUCAAUCGCGAAGAGCCCACUGGGAGCGGAGC-3’

15nt-KL B-Pepper: > 5’-
GGGACGAGGGUCGGCAAGUCGACAGCUGACCCUCGUCCCAAGGCUGACCAAUCGUGGCG
UGUCGGCAGAGCAAGUCGACAGCUCUGCACUGGCGCCGUCAGCCAAGCGCUCGCCCUCGC
CAAGUCGACAGGUGAGGGCGAGUGC-3’

15nt-KL C-Mango: > 5’-
GCUCGAUUGACGGGCAAGGUACCAGCCCGUCAAUCGAGCAACCUAGCGGCUUACUCAAG
GUACCAGGGUAGGCUGCUAGGAAGCGCCAUUCAUUGUAAAGGUACCAUACAAUGAGUG
GCGCAAGGCACGUACGAAGGAGAGGAGAGGAAGAGGAGAGUACGUGCC-3’

MS2 Aptamer Constructs (for Protein Recruitment)

15nt-KL A-Broccoli-MS2: > 5’-
GCGAGAGCGCUGCCCAAUCGCGAAGGGCAGCGCUCUCGCAAGGAUGGACGGUCGGGUCC
GAGGGCAAUCGCGAAGCCCUCGUCGAGUAGAGUGUGGGCCAUCCAAGCGUUCACACUGA
CCAAUCGCGAAGGUCAGUGUGAACGCAAACAUGAGGAUCACCCAUGU-3’

- MS2 aptamer (3’ appended): AAACAUGAGGAUCACCCAUGU

15nt-KL B-Broccoli-MS2: > 5’-
GCGAGAGCGCUGCCCAAGUCGACAGGGCAGCGCUCUCGCAAGGAUGGACGGUCGGGUCC
GAGGGCAAAGUCGACAGCCCUCGUCGAGUAGAGUGUGGGCCAUCCAAGCGUUCACACUG
ACCAAGUCGACAGGUCAGUGUGAACGCAAACAUGAGGAUCACCCAUGU-3’

15nt-KL WT-Broccoli-MS2: > 5’-
GCGAGAGCGCUGCCCAAGCGCGCAGGGCAGCGCUCUCGCAAGGAUGGACGGUCGGGUCC
GAGGGCAAGCGCGCAGCCCUCGUCGAGUAGAGUGUGGGCCAUCCAAGCGUUCACACUGA
CCAAGCGCGCAGGUCAGUGUGAACGCAAACAUGAGGAUCACCCAUGU-3’

Orthogonal Set for Multiplexing

15nt-KL WT-Pepper: > 5’-
GGGACGAGGGUCGGCAAGCGCGCAGCUGACCCUCGUCCCAAGGCUGACCAAUCGUGGCG
UGUCGGCAGAGCAAGCGCGCAGCUCUGCACUGGCGCCGUCAGCCAAGCGCUCGCCCUCGC
CAAGCGCGCAGGUGAGGGCGAGUGC-3’

15nt-KL B-Mango: > 5’-
GCUCGAUUGACGGGCAAGUCGACAGCCCGUCAAUCGAGCAACCUAGCGGCUUACUCAAG
UCGACAGGGUAGGCUGCUAGGAAGCGCCAUUCAUUGUAAAGUCGACAUAUAAUGAGUG
GCGCAAGGCACGUACGAAGGAGAGGAGAGGAAGAGGAGAGUACGUGCC-3’

15nt-KL E-Mango: > 5'-
GCGAGAGCGCUGCCCAAGUAUACAGGGCAGCGCUCUCGCAAGCGAUGAACGUAGGGAAG
UAUACACCCUACGUUCAUCGCAAGCGUUCACACUGACCAAGUAUACAGGUCAGUGUGA
ACGCAAGGCACGUACGAAGGAGAGGAGAGGAAGAGGAGAGUACGUGCC-3'

15nt-KL F-Mango: > 5'-
GCUCGAUUGACGGGCAAAAUAUAUAGCCCGUCAAUCGAGCAACCUAGCGGCUUACUCAA
AAUAUAUAGGGUAGGCUGCUAGGAAGCGCCAUUCAUUGUAAAAAUAUAUAUACAAUGA
GUGGCGCAAGGCACGUACGAAGGAGAGGAGAGGAAGAGGAGAGUACGUGCC-3'

Linker Nanostars (for Sub-compartmentalization)

15nt-KL AB-Linker-2arm: > 5'-
GCGAGAGCGCUGCCCAAUCGCGAAGGGCAGCGCUCUCGCAAGCGAUGAACGUAGGGAAG
UCGACACCCUACGUUCAUCGC-3'

15nt-KL AB-Linker-4arm-Broccoli: > 5'-
GCGAGAGCGCUGCCCAAUCGCGAAGGGCAGCGCUCUCGCAAGGAUGGACGGUCGGGUCC
GAGGGCAAUCGCGAAGCCCUCGUCGAGUAGAGUGUGGGCCAUCAAGCGUUCACACUGAC
CAAGUCGACAGGUCAGUGUGAACGCAAGAUGUAUUCAAGUCCAAGUCGACAGGGCUUG
AGUACGUC-3'

Aptamer Sequences

Aptamer	Sequence (5'-3')	Ligand	Color
Broccoli	AGAGCGCUGCCCAAGACUGA	DFHBI-1T (40 uM)	Green
Pepper	CCGGGACCAUCGUGGCGUGUCGGCAG	HBC530 (10 nM)	Red
Mango	AAGCGAUGAACGUAGGG	TO1-biotin (200 nM)	Yellow
MS2	AAACAUGAGGAUCACCCAUGU	MCP-mCherry fusion	N/A

Tornado Ribozyme Sequences

5' Twister ribozyme: > 5'-
GAGGGCCUAUUUCCCAUGAUUCCUUCAUAUUUGCAUAUGCUUACCGUAACUUGAAAGU
AUUUCGAUUUCUUG-3'

3' Twister ribozyme: > 5'-
GCUUUAUAUAUCUUGUGGAAAGGACGAAACACCGUGCUCGCUUCGGCAGCACAUACUA
CUGACUGGCCGCACUCGCCGGUCCCAAGCCCGGAUAAAAUGGGAGGGGGCGGGAAACCG
CCU-3'

DNA Insert Sequences (Template Strand)

Representative DNA template sequences for key constructs (used for oligonucleotide synthesis):

15nt-KL A-Broccoli (coding strand): > 5'-
GCGAGAGCGCTGCCCAATCGCGAAGGGCAGCGCTCTCGCAAGGATGGACGGTCGGGTCCG

AGGGCAATCGCGAAGCCCTCGTCGAGTAGAGTGTGGGCCATCCAAGCGTTCACACTGACC
AATCGCGAAGGTCAGTGTGAACGC-3’

15nt-KL A-MS2 (coding strand): > 5’-
GCGAGAGCGCTGCCCAATCGCGAAGGGCAGCGCTCTCGCAAGGATGGACGGTCGGGTCCG
AGGGCAATCGCGAAGCCCTCGTCGAGTAGAGTGTGGGCCATCCAAGCGTTCACACTGACC
AATCGCGAAGGTCAGTGTGAACGCAAACATGAGGATCACCCATGT-3’

Plasmid Maps and Cloning Details

All nanostar sequences were cloned into pAV-U6+27-Tornado-Broccoli (Addgene #124360) using NotI-HF and SacII restriction sites. Cloning protocol: 1. Digest vector with NotI-HF (NEB R3189S, 2 uL per 20 uL reaction) and SacII (NEB R0157S) 2. Phosphorylate double-stranded oligonucleotide inserts (IDT) with T4 PNK 3. Insert strands were annealed (95 degC 2 min, cool to 25 degC at 1 degC/s) 4. Ligate with T4 DNA ligase (NEB M0202S) at 16 degC the night 5.Transform into DH5alpha competent cells (ThermoFisher EC0112) 6. Verify by whole-plasmid sequencing (Eurofins Genomics)

Supplementary Note 2: Mathematical Model of Condensate-Mediated Gene Regulation

We developed a minimal compartment model to understand how RNA condensate formation influences local effector concentration at genomic target sites and to predict the relationship between monomer concentration and transcriptional output.

Two-state compartment model. The system is described by a two-state equilibrium between dispersed monomers (state D) and condensed droplets (state C). Monomers in the dispersed phase have concentration $[M]_{disp}$ and are available for dCas9 binding and chromatin targeting. Monomers partitioned into condensates have an effective local concentration [M]cond that exceeds the dispersed-phase concentration by a partition coefficient P = [M]cond/[M]disp. The total monomer concentration [M]tot is conserved: [M]tot = fdisp[M]disp + fcond[M]cond, where fdisp and fcond are the volume fractions of each phase.

Critical concentration and supersaturation. Condensate formation occurs when $[M]_{tot}$ exceeds a critical concentration C*, which depends on the KL interaction strength, the number of valencies per monomer, and solution conditions (salt, temperature, crowding agents). For KL-A nanostars, C* ~ 50 nM in physiological buffer; for KL-WT, C* ~ 200 nM. Above C*, the excess monomer partitions into the condensed phase according to a lever rule. Within condensates, local monomer concentrations reach 5-25 uM, corresponding to a supersaturation ratio of 10-50x relative to the dispersed phase at comparable total concentrations.

Concentration enhancement at chromatin. The functional output of the system depends on the concentration of dCas9-sgRNA-nanostar-target complexes at the genomic locus. We estimate the concentration enhancement as follows. In the dispersed regime ([M]tot < C), target-bound complexes have concentration [Bound]disp = [M]tot . [dCas9] . Ka / (Kd + [M]tot), where Ka is the association constant for dCas9-sgRNA binding and Kd is the dissociation constant from chromatin. In the condensed regime, monomers released from condensate surfaces contribute an additional term [Bound]cond = P . fsurf . [M]cond . gamma . Ka / Kd, where fsurf is the surface-accessible fraction and gamma accounts for the enhanced rebinding probability due to reduced diffusion dimensionality near the condensate-chromatin interface. The total concentration enhancement at the locus is the ratio ([Bound]disp + [Bound]cond) / [Bound]disp evaluated at the same [M]tot.

Hill-function mapping to transcriptional output. The local effector concentration feeds into a Hill function describing transcriptional response: $F_{output} = F_{max} . [Bound]^n / (K_M^n + [Bound]^n)$, where F_{max} is the maximum activation or repression fold, K_M is the half-maximal concentration, and n is the Hill coefficient. With the condensate-mediated enhancement of [Bound], the apparent K_M is reduced by the same factor, shifting the dose-response curve to lower input concentrations. This prediction was supported by the dose-dependent EGFP activation observed at increasing nanostar inputs (Supplementary Fig. 7).

Supplementary Note 3: Statistical Methods

Multiple testing correction. When we conducted the same assay for several genes, time points or conditions, we adjusted the false discovery rate (FDR) by the Benjamini-Hochberg method. To control family-wise error rate for the prespecified comparisons, the Holm-Bonferroni step-down procedure was applied. For Fig. 2b (which includes 15 pairwise comparisons: 5 systems × 3 genes), Bonferroni correction was applied, and significance was set at $P < 0.0033$ for an alpha of 0.05, and all significant differences reported were still significant after correction. The choice of correction method was specified in each figure legend.

Image analysis pipeline. Confocal microscopy images were processed using a custom Fiji/ImageJ macro pipeline. Briefly: (1) flat-field correction using a median-of-stack illumination reference, (2) rolling-ball background subtraction (radius = 50 pixels), (3) 3D median filtering (kernel size 3 x 3 x 3), (4) adaptive thresholding using the Phansalkar method (radius = 15 pixels, $k = 0.25$), and (5) watershed segmentation for overlapping condensates. Condensate masks were filtered by size (0.1-10 um^3) and sphericity (>0.5) to exclude debris and out-of-focus artifacts.

Intensity measurements were extracted from raw unprocessed images using the segmented masks to avoid bias from filtering operations. For colocalization analysis, Pearson's correlation coefficient (PCC) was calculated on background-subtracted images within manually defined nuclear regions of interest. PCC values were computed using the Coloc2 plugin with Costes thresholding and automatic PSF estimation. All image analyses were performed blinded to experimental condition where possible.

Software and reproducibility. Analysis was performed using GraphPad Prism 10, R (v4.3), and Python (SciPy 1.11). The exact P values are reported in the figure legends; the value of $P < 0.0001$ is represented when a P value is less than 0.0001. Error bars on graphs represent standard deviation unless otherwise indicated. All experiments were performed with a minimum of three biological replicates (independent transfections or cell passages). No data points were excluded unless technical failure was documented (for example, pipetting error, cell death before imaging).

Supplementary Figures

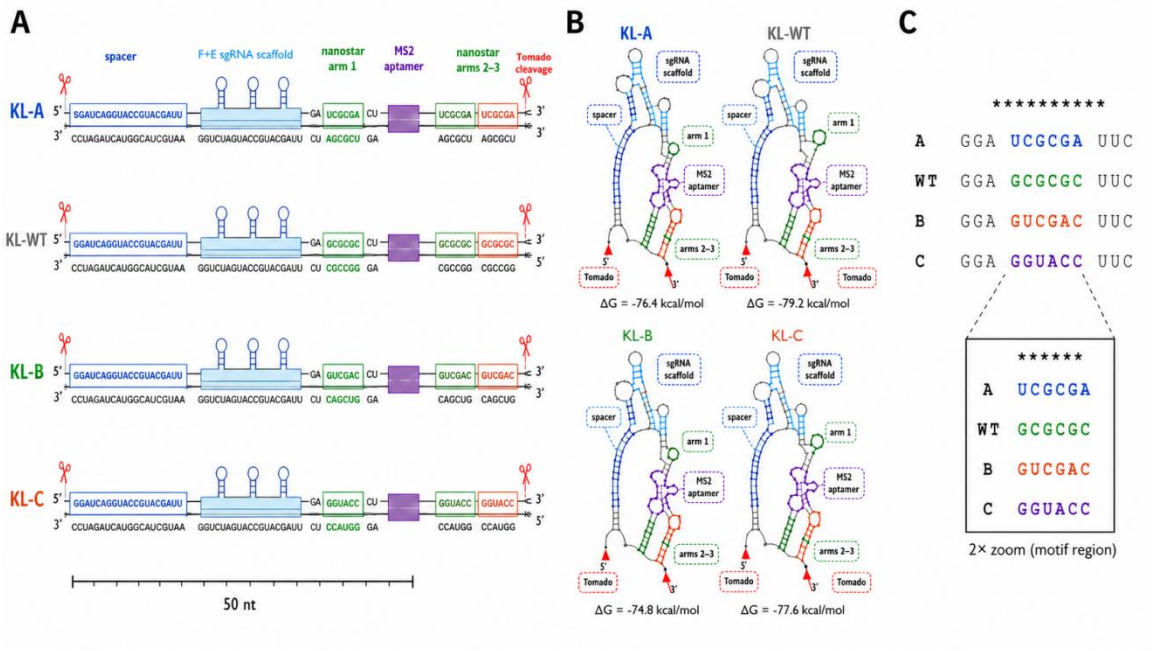

Supplementary Fig. 1 | Full sequence maps of sgRNA-nanostar chimeras. A, Linear sequence maps showing the organization of domains from 5' to 3': spacer region, F+E sgRNA scaffold, nanostar arm 1, aptamer core, nanostar arms 2-3, and Tornado cleavage sites. KL variants A, WT, B, and C are indicated by color. B, Predicted minimum free energy secondary structures for each chimera, annotated with domain boundaries. C, Sequence alignment of the four KL variants highlighting the six-nucleotide recognition motif.

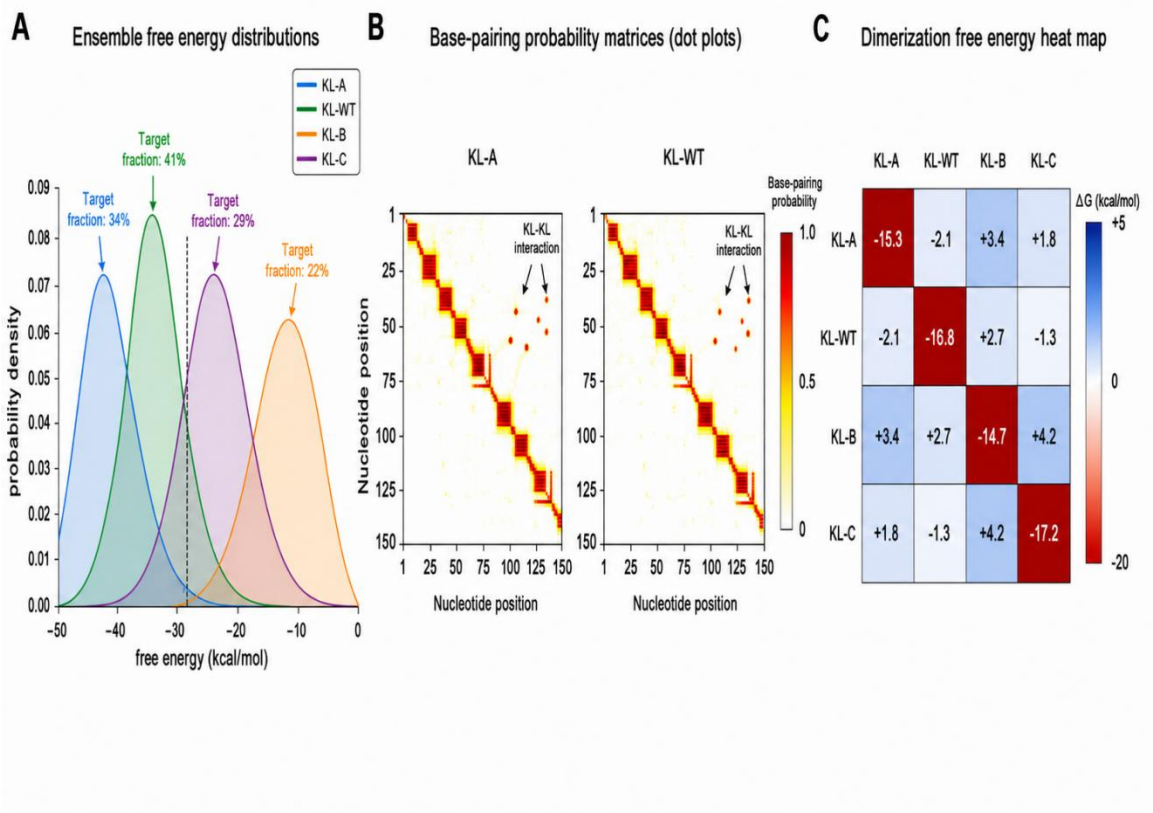

Supplementary Fig. 2 | NUPACK-predicted secondary structures. A, Ensemble free energy distributions for each nanostar design, showing the target structure fraction within the Boltzmann ensemble. B, Base-pairing probability matrices (dot plots) for KL-A and KL-WT nanostars, showing strong on-diagonal pairing in stem regions and off-diagonal KL-KL interaction probabilities. C, Predicted dimerization free energies for all pairwise KL combinations, arranged as a heat map.

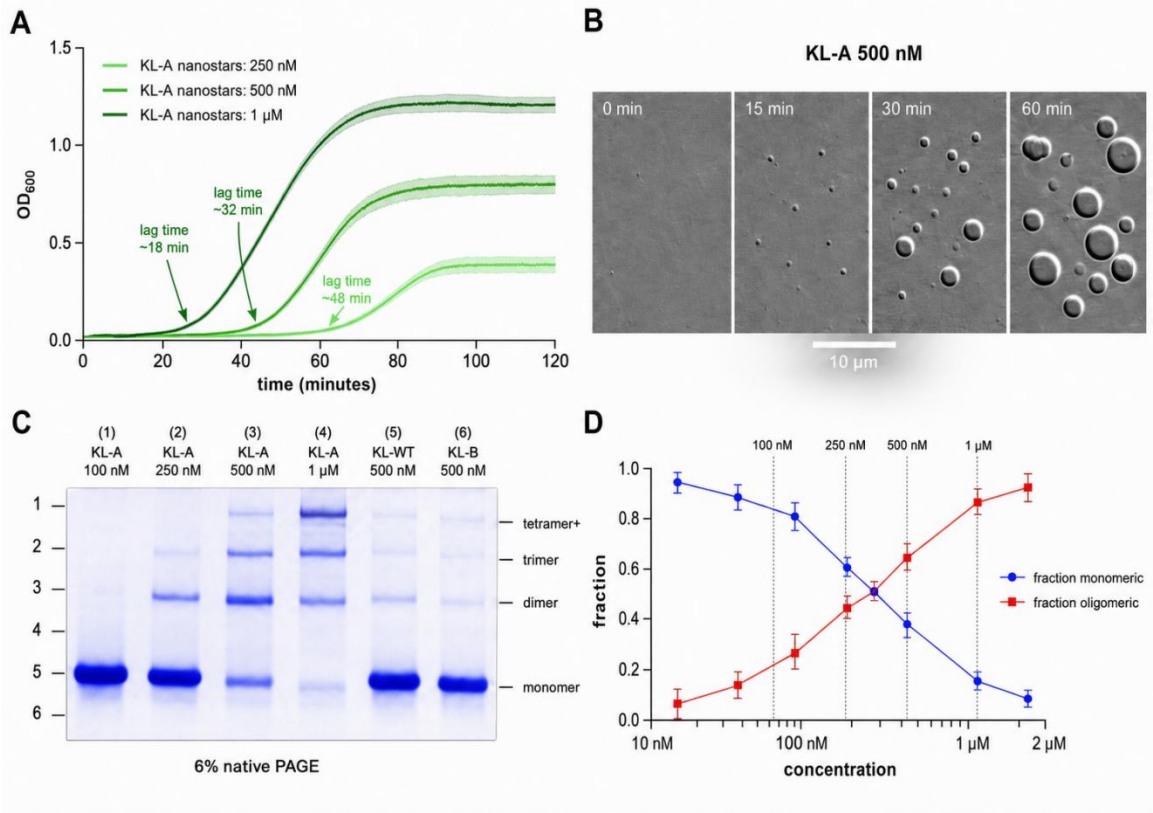

Supplementary Fig. 3 | In vitro condensate formation time course and PAGE analysis. A, Turbidity (OD_{600}) measurements over 120 min for KL-A nanostars at 250 nM, 500 nM, and 1 uM, showing sigmoidal assembly kinetics. B, Representative DIC images at 0, 15, 30, and 60 min for KL-A at 500 nM. C, Native PAGE (6%) showing monomer, dimer, and higher-order species for KL-A, KL-WT, and KL-B nanostars at indicated concentrations. D, Quantification of band intensities showing the fraction in monomeric versus oligomeric species as a function of concentration. Scale bar, 10 um.

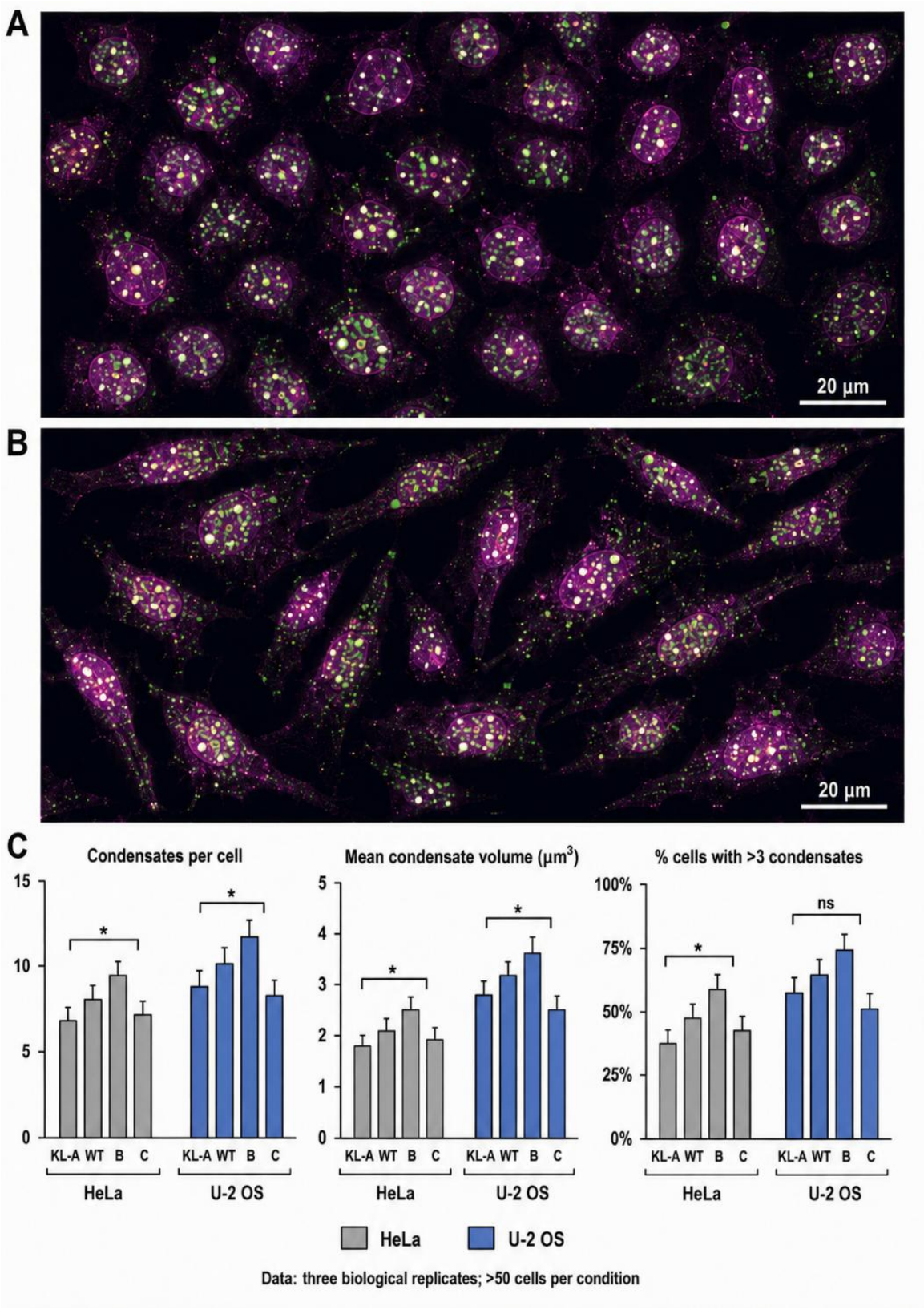
A
20 µm
B
20 µm
C
Condensates per cell
Mean condensate volume (µm3)
% cells with >3 condensates
15
10
5
0
5
4
3
2
1
0
100%
75%
50%
25%
0%
*
*
*
*
*
ns
KL-A WT B C
KL-A WT B C
HeLa
U-2 OS
HeLa
U-2 OS
HeLa
U-2 OS
HeLa
U-2 OS
Data: three biological replicates; >50 cells per condition

Supplementary Fig. 4 | Condensate formation in HeLa and U-2 OS cells (full fields). A, Representative full-field confocal images of HeLa cells expressing KL-A nanostars (Broccoli-DFHBI, green) and dCas9-NLS-mCherry (magenta). B, Corresponding images in U-2 OS cells. C, Quantification of condensate number per cell, mean condensate volume, and fraction of cells with condensates (>3 foci) for both cell lines across all four KL variants. Data are from three biological replicates with >50 cells per condition. Scale bars, 20 um.

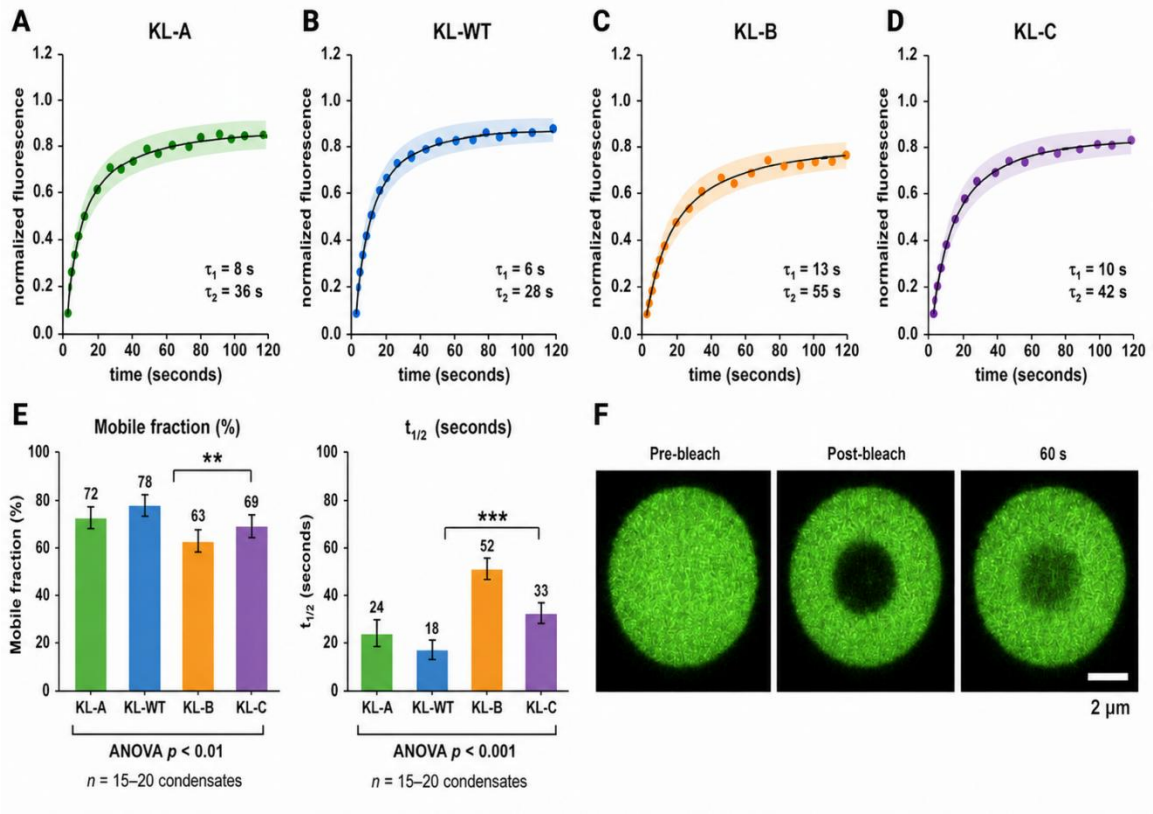

Supplementary Fig. 5 | Extended FRAP data for all nanostar variants. A-D, Normalized FRAP curves for KL-A (A), KL-WT (B), KL-B (C), and KL-C (D) condensates in HEK293T cells. Solid lines are biexponential fits; shaded areas are 95% confidence intervals. E, Mobile fraction and half-time of recovery (t1/2) for each variant. F, Representative pre-bleach, bleach, and recovery frames for KL-A condensates. Scale bar, 2 um.

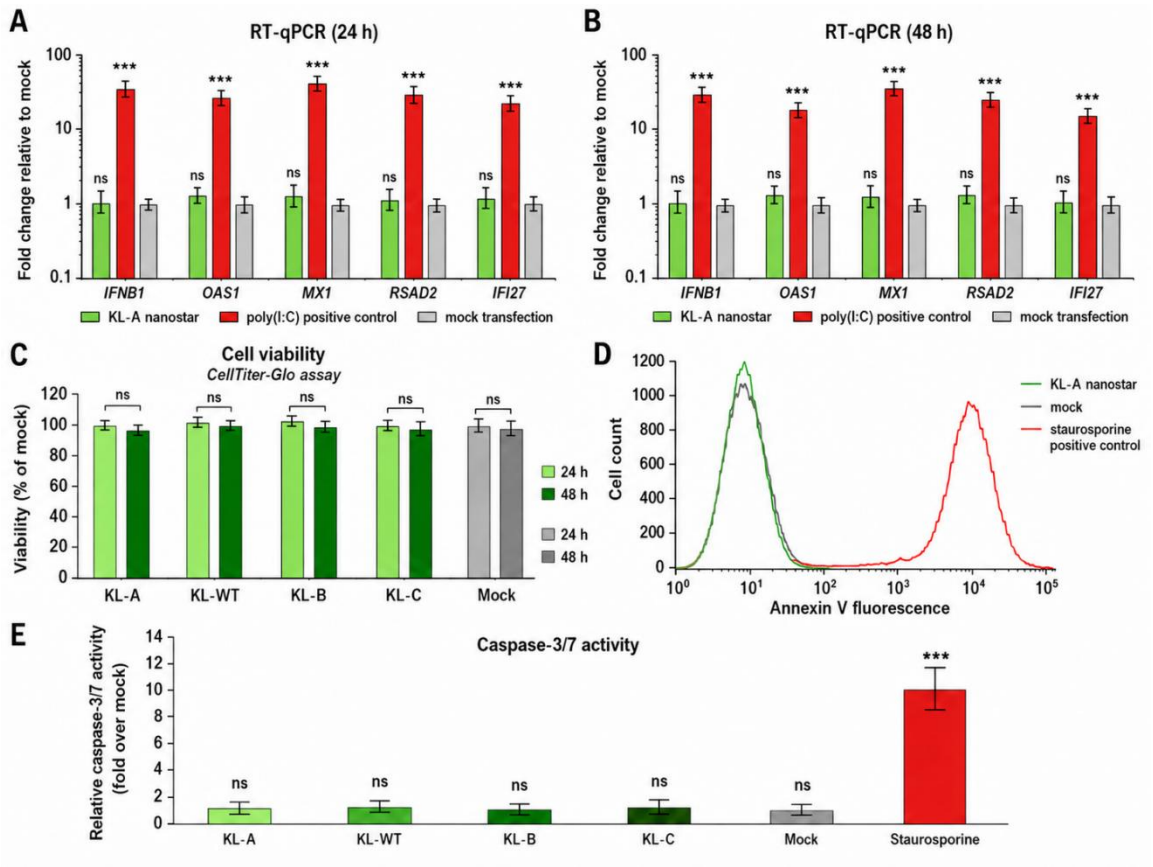

Supplementary Fig. 6 | Extended immune response qPCR and cell viability data. A, RT-qPCR for IFNB1, OAS1, MX1, RSAD2, and IFI27 in HEK293T cells at 24 h posttransfection with KL-A nanostars, poly(I:C) (positive control), or mock transfection. B, Same assays at 48 h. C, Cell viability (CellTiter-Glo) for all nanostar variants at 24 and 48 h. D, Annexin V staining by flow cytometry at 48 h. E, Caspase-3/7 activity as a percentage of staurosporine-treated positive control. Data are mean +/- s.d. from three biological replicates.

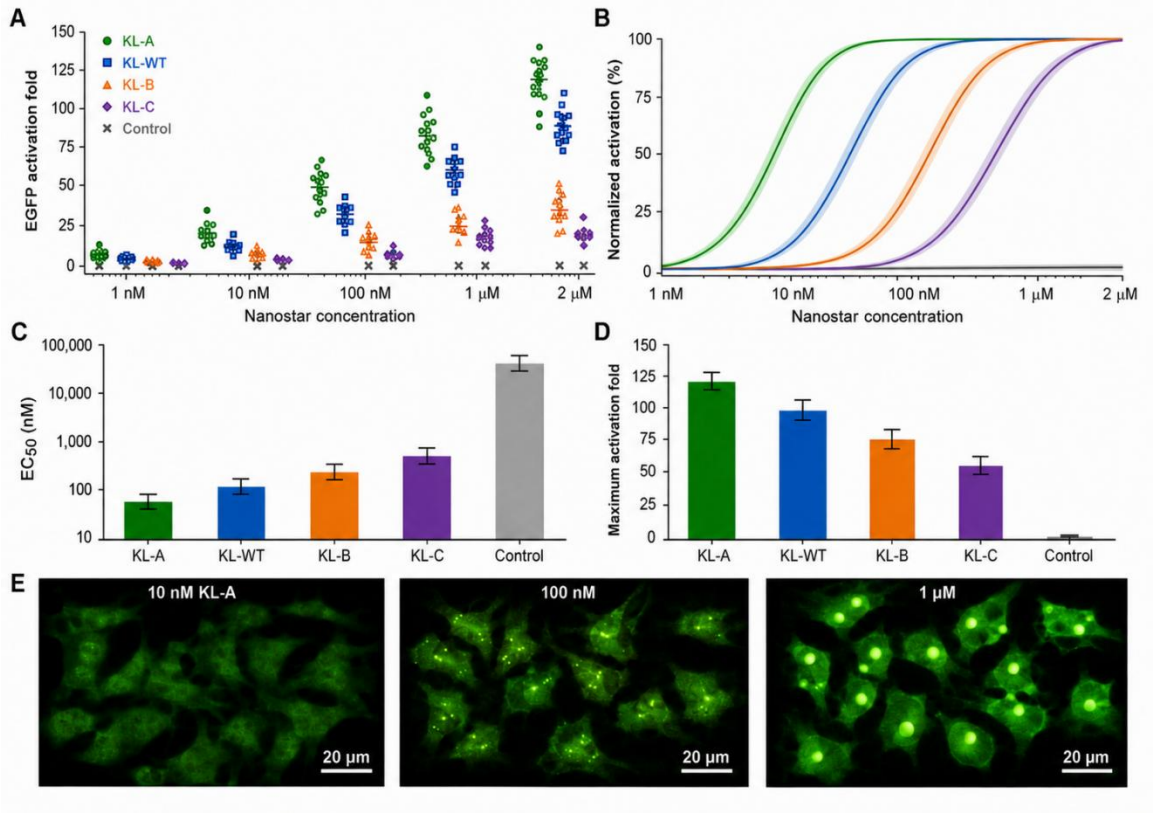

Supplementary Fig. 7 | Dose-response replicate data and EC_{50} curves. A, EGFP activation fold at increasing nanostar concentrations (1 nM to 2 uM) for KL-A, KL-WT, KL-B, KL-C, and non-condensing controls. Each data point represents an independent biological replicate. B, Fitted four-parameter logistic curves with 95% confidence bands. C, EC_{50} values for each variant derived from logistic fits. D, Maximum activation fold (E_{max}) comparison across variants. E, Representative images at 10 nM, 100 nM, and 1 uM for KL-A. Scale bar, 20 um.

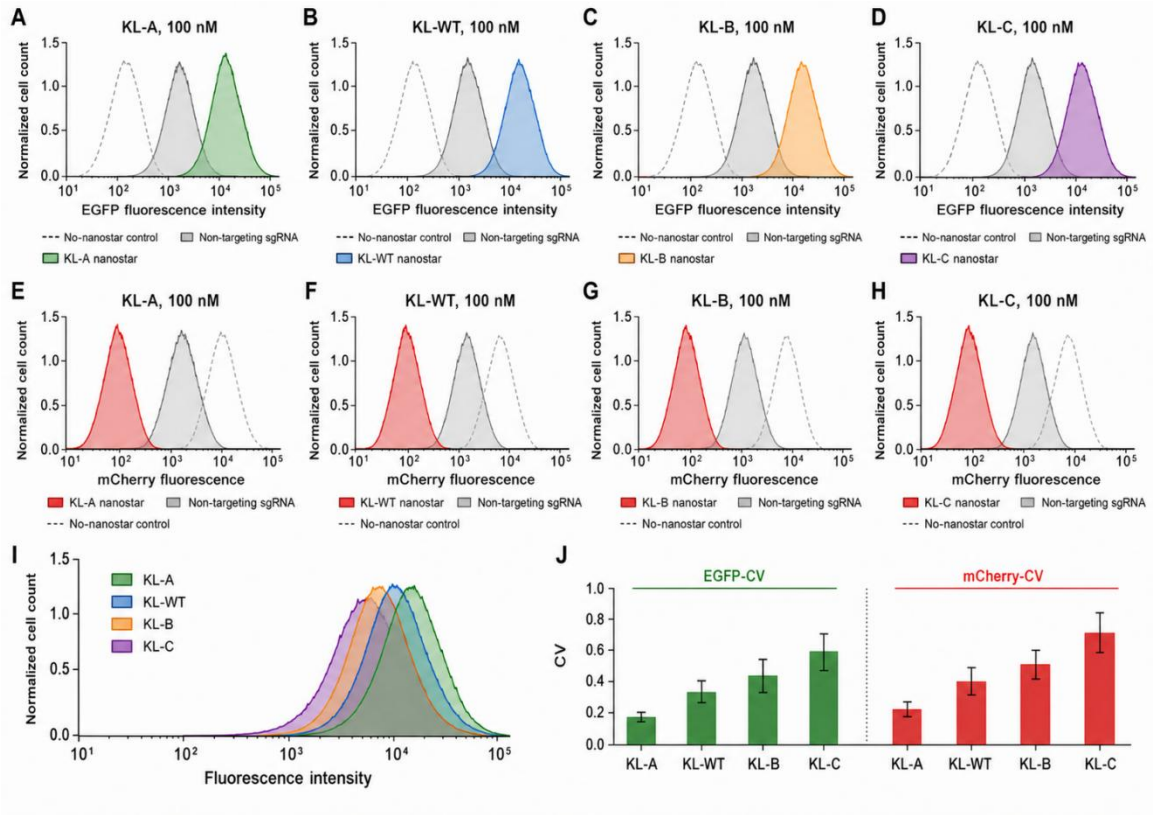

Supplementary Fig. 8 | Single-cell flow cytometry histograms for all conditions. a-d, Fluorescence intensity distributions for EGFP (activation) in cells treated with KL-A (A), KL-WT (B), KL-B (C), or KL-C (D) nanostars at 100 nM, compared to non-targeting sgRNA and no-nanostar controls. E-H, Corresponding distributions for mCherry (repression) under the same conditions. I, Overlay histograms comparing all KL variants at 100 nM. J, Coefficient of variation (CV) for each condition as a measure of cell-to-cell heterogeneity.

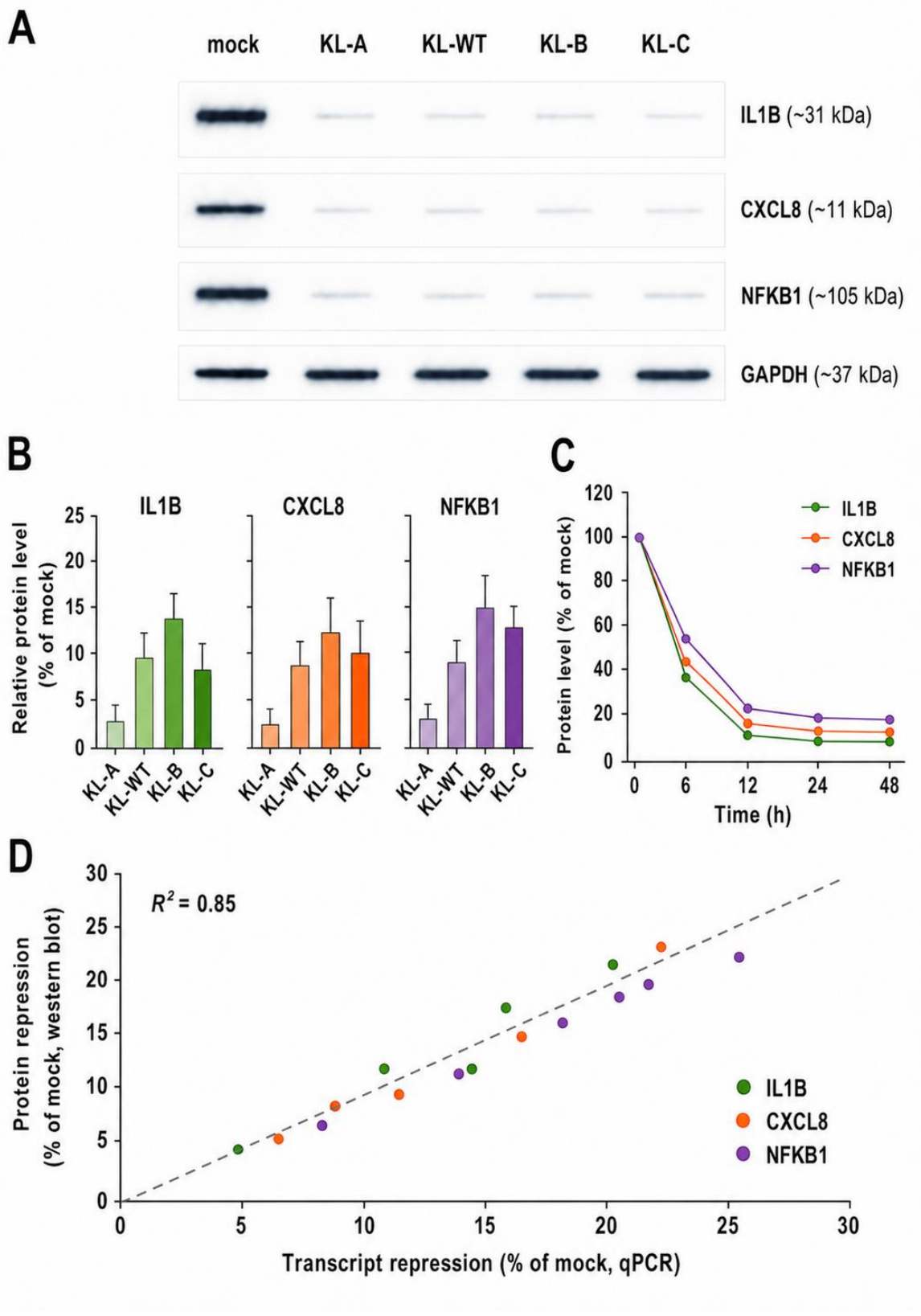
A
mock
KL-A
KL-WT
KL-B
KL-C
IL1B (~31 kDa)
CXCL8 (~11 kDa)
NFKB1 (~105 kDa)
GAPDH (~37 kDa)
B
IL1B
CXCL8
NFKB1
Relative protein level (% of mock)
KL-A
KL-WT
KL-B
KL-C
C
Protein level (% of mock)
Time (h)
IL1B
CXCL8
NFKB1
D
R^2 = 0.85
Protein repression (% of mock, western blot)
Transcript repression (% of mock, qPCR)
IL1B
CXCL8
NFKB1

Supplementary Fig. 9 | Western blot analysis of repression targets (full panel). A, Full western blot images for IL1B, CXCL8, and NFKB1 in HEK293T cells following CRISPR-condensate repression with each KL variant. B, Quantification of band intensities normalized to GAPDH loading control. C, Time course of protein-level repression (0, 6, 12, 24, 48 h) for KL-A nanostars. D, Comparison of transcript-level (qPCR) and protein-level (western) residual transcript and protein levels, expressed as percentages of the mock control at 24 h for all three targets.

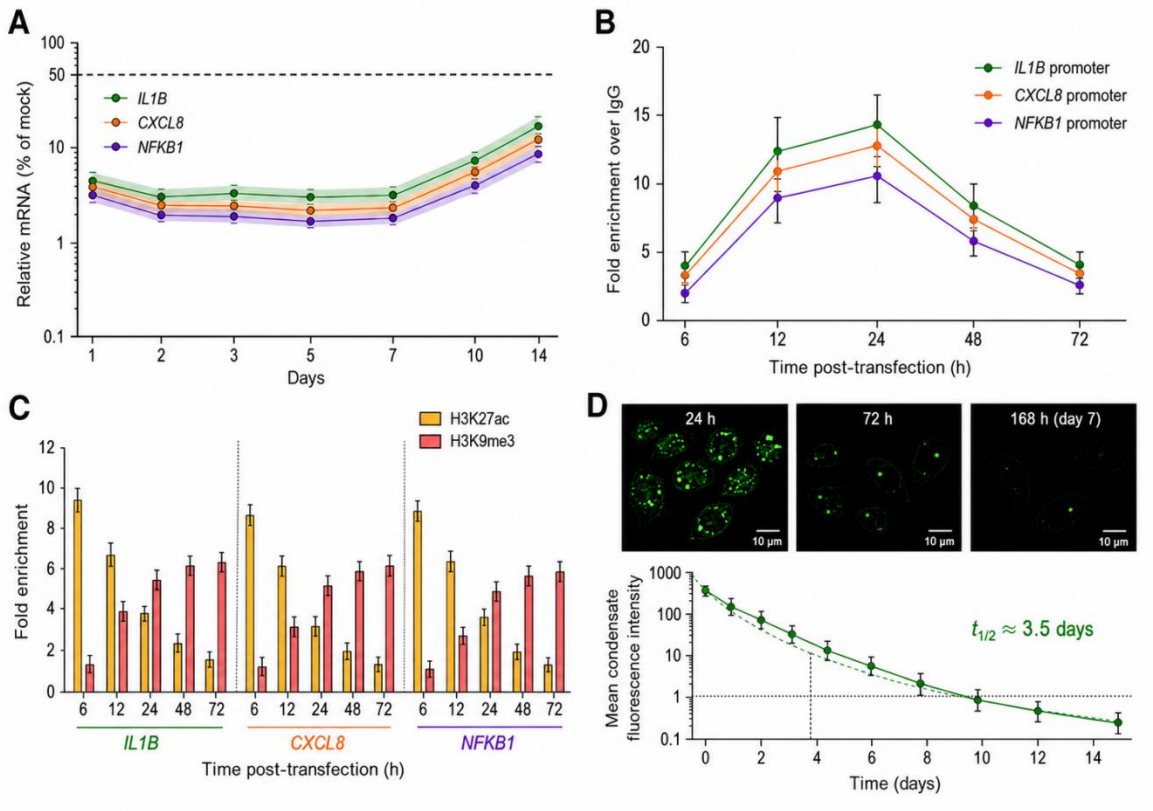

Supplementary Fig. 10 | Long-term repression stability and ChIP time course. A, RT-qPCR of IL1B, CXCL8, and NFKB1 following KL-A nanostars transient transfection at days 1, 2, 3, 5, 7, 10, and 14. B, ChIP-qPCR for dCas9 occupancy at the IL1B, CXCL8, and NFKB1 promoters 6, 12, 24, 48 and 72 h post-transfection. C, ChIP-qPCR for H3K27ac and H3K9me3 at the same time points at the IL1B, CXCL8, and NFKB1 loci. D, Condensate persistence measured by Broccoli fluorescence at paired time points. Results are mean +/- s.d. from three biological replicates.

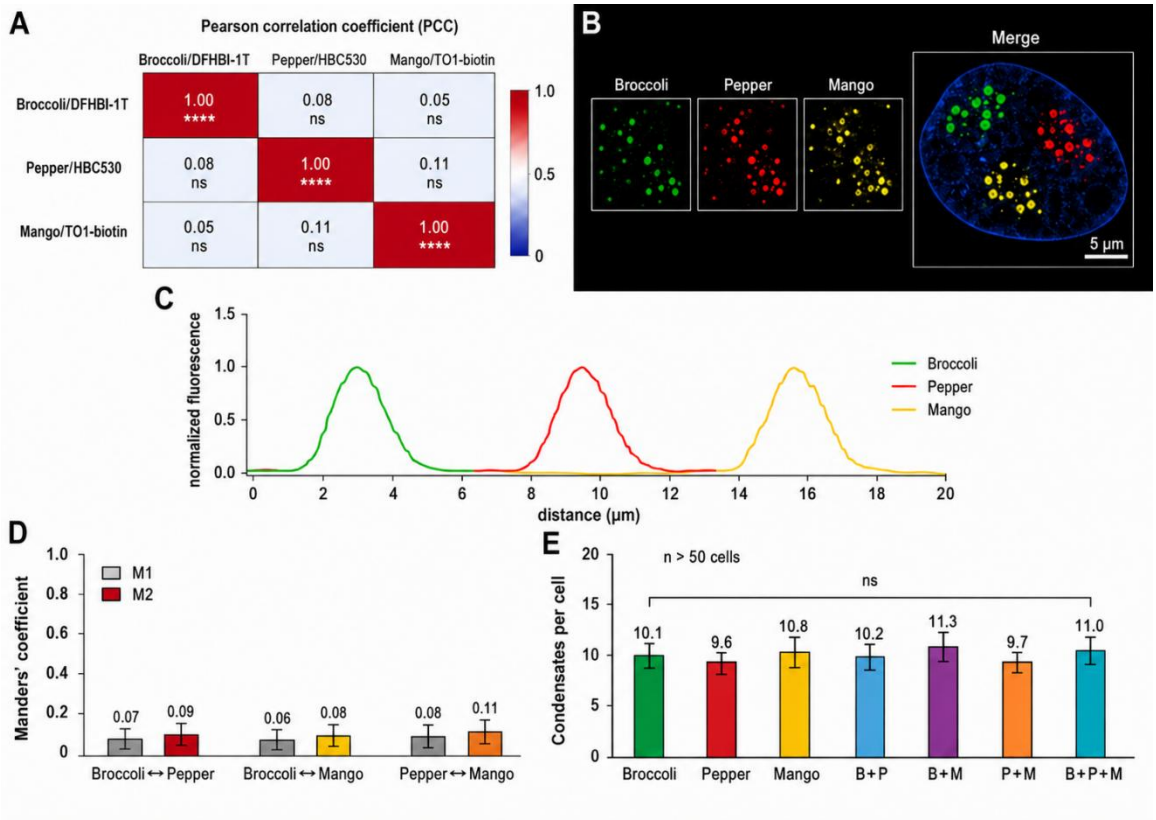

Supplementary Fig. 11 | Orthogonal condensate full PCC matrix and three-color imaging. A, Complete pairwise Pearson correlation matrix for all channel combinations in three-color imaging experiments (Broccoli/DFHBI-1T, Pepper/HBC530, Mango/TO1-biotin). B, Representative three-color images showing the spatial organization of orthogonal condensates in HEK293T nuclei. C, Line scan intensity profiles across a three-color condensate showing internal partitioning. D, Manders' M1 and M2 coefficients for all pairwise comparisons. E, Quantification of condensate number per cell for each orthogonal combination. Scale bars, 5 um.

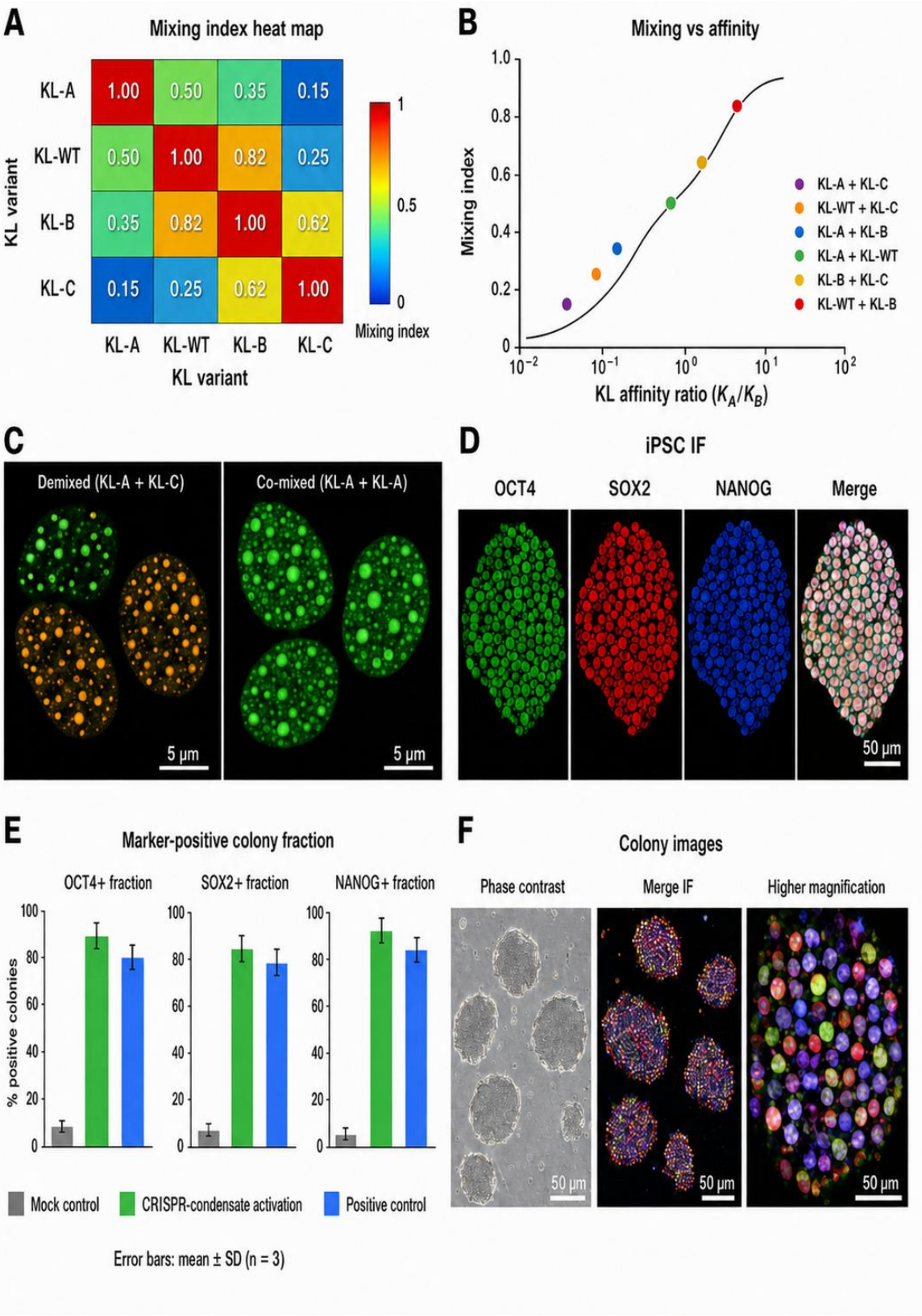
A
Mixing index heat map
KL-A
KL-WT
KL-B
KL-C
1.00
0.50
0.35
0.15
0.50
1.00
0.82
0.25
0.35
0.82
1.00
0.62
0.15
0.25
0.62
1.00
KL variant
KL-A
KL-WT
KL-B
KL-C
KL variant
1
0.5
0
Mixing index
B
Mixing vs affinity
Mixing index
1.0
0.8
0.6
0.4
0.2
0
10^{-2}
10^{-1}
10^{0}
10^{1}
10^{2}
KL affinity ratio (K_A/K_B)
KL-A + KL-C
KL-WT + KL-C
KL-A + KL-B
KL-A + KL-WT
KL-B + KL-C
KL-WT + KL-B
C
Demixed (KL-A + KL-C)
Co-mixed (KL-A + KL-A)
5 µm
5 µm
D
iPSC IF
OCT4
SOX2
NANOG
Merge
50 µm
E
Marker-positive colony fraction
OCT4+ fraction
SOX2+ fraction
NANOG+ fraction
% positive colonies
100
80
60
40
20
0
Mock control
CRISPR-condensate activation
Positive control
Error bars: mean ± SD (n = 3)
F
Colony images
Phase contrast
Merge IF
Higher magnification
50 µm
50 µm
50 µm

Supplementary Fig. 12 | Sub-compartmentalization mixing indices and iPSC immunofluorescence. A, Mixing indices (1 - $|I_A - I_B| / (I_A + I_B)$) for all pairwise KL variant combinations, indicating the degree of sub-compartmentalization versus co-mixing. B, Mixing index as a function of the KL affinity ratio between components. C, Representative images of demixed (KL-A + KL-C) and co-mixed (KL-A + KL-A) condensates. D, Immunofluorescence for POU5F1 (OCT4), SOX2, and NANOG in iPSCs following CRISPR-condensate treatment. E, Quantification of marker-positive colony fractions. F, Representative phase-contrast and immunofluorescence images of iPSC colonies. Scale bars, 50 um.

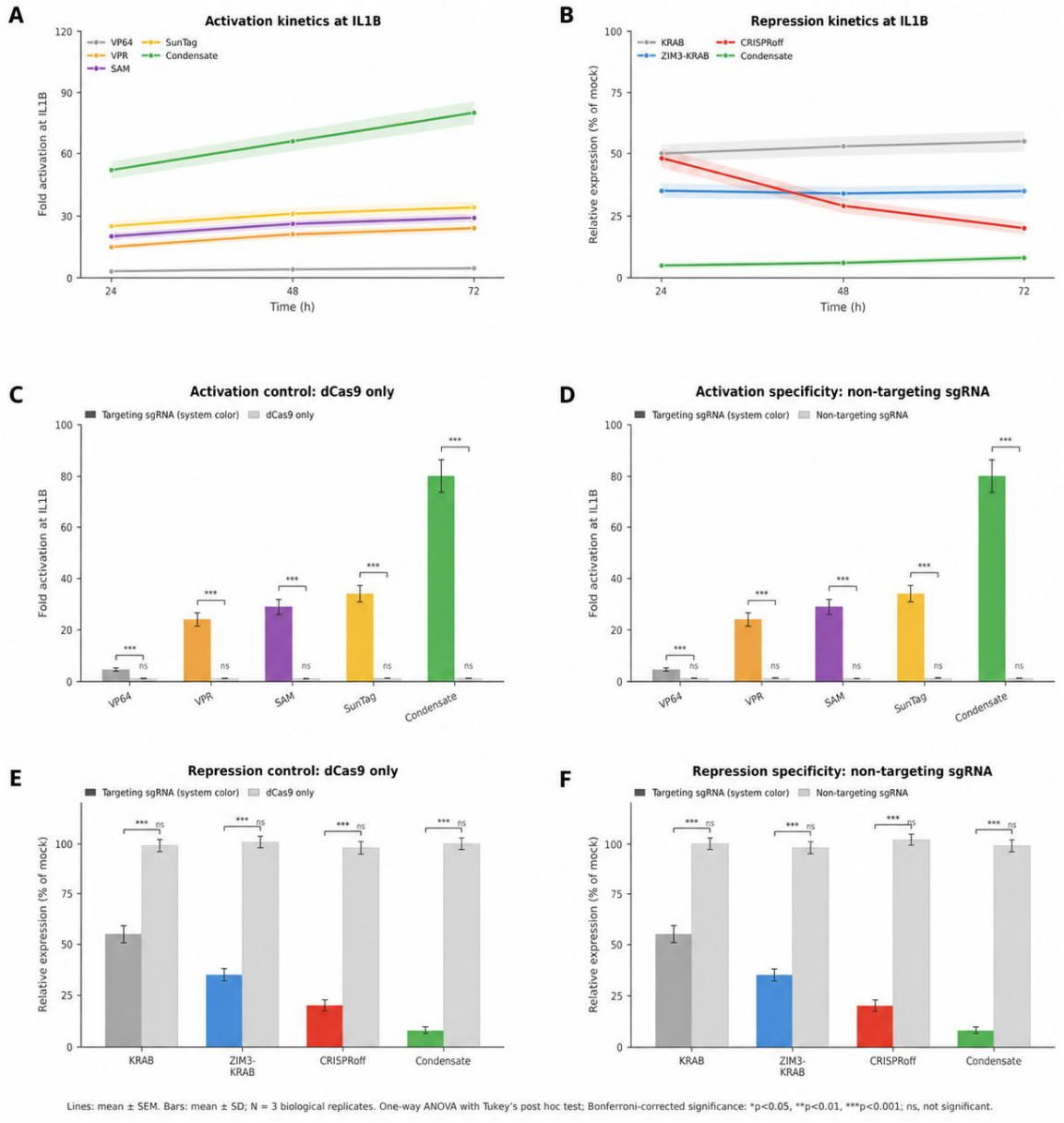

Supplementary Fig. 13 | Multi-timepoint activation and repression kinetics with negative controls. A, Activation time course at IL1B over 24, 48, and 72 h comparing all five systems (VP64, VPR, SAM, SunTag, Condensate). B, Repression

time course at IL1B over 24, 48, and 72 h comparing all four systems (KRAB, ZIM3-KRAB, CRISPRoff, Condensate). C, dCas9-only control (without sgRNA) for activation, showing baseline levels of 1.0-1.5-fold for all systems. D, Non-targeting sgRNA control for activation, confirming specificity. E, dCas9-only control for repression. F, Non-targeting sgRNA control for repression. All controls confirm that observed effects are support the conclusion that the observed regulatory effects are sgRNA-dependent. Data are mean +/- s.d. from N = 3 biological replicates.

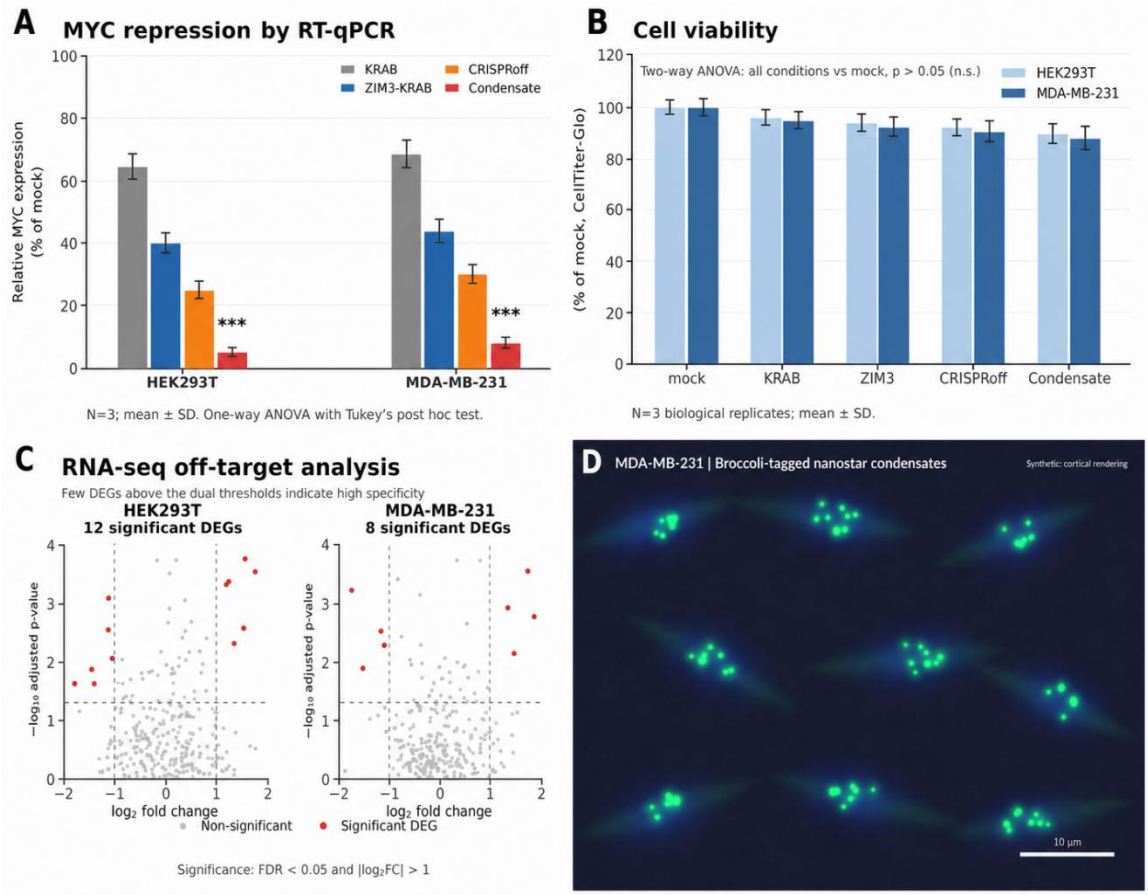

Supplementary Fig. 14 | CRISPR-Condensate validation in MDA-MB-231 triple-negative breast cancer cells. A, RT-qPCR comparing MYC residual transcript and protein levels, expressed as percentages of the mock control between HEK293T and MDA-MB-231 cells across all four repression systems (KRAB, ZIM3-KRAB, CRISPRoff, Condensate). B, Cell viability (CellTiter-Glo) at 48 h for all conditions in MDA-MB-231 cells. C, transcriptome-wide differential expression analysis: volcano plot showing DEGs in MDA-MB-231 cells following Condensate-mediated MYC repression. D, Representative confocal images of Broccoli-tagged nanostar condensates in MDA-MB-231 cells showing comparable condensate formation to HEK293T. Scale bar, 10 um. Data are mean +/- s.d. from N = 3 biological replicates.

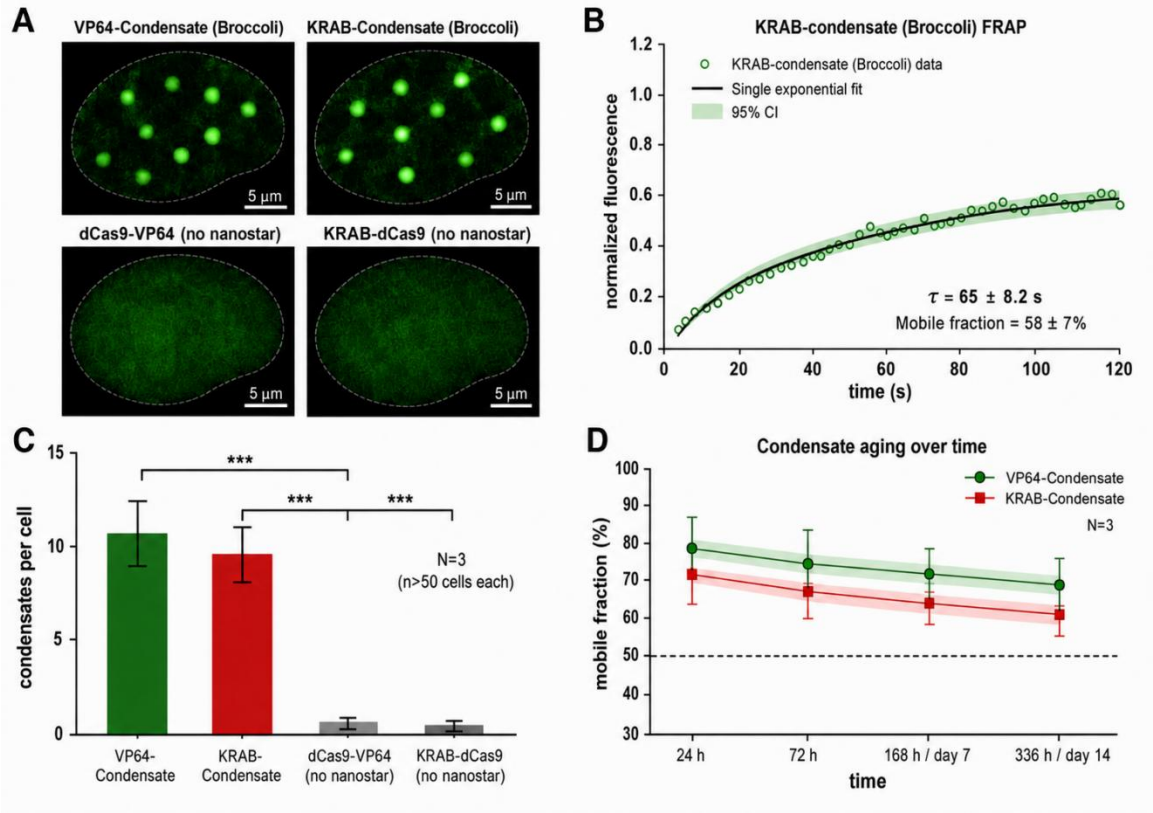

Supplementary Fig. 15 | Traditional CRISPR system condensate controls and KRAB condensate characterization.A, Representative confocal images: VP64-Condensate (Broccoli, green puncta), KRAB-Condensate (Broccoli, green puncta), dCas9-VP64 no nanostar (diffuse, no puncta), KRAB-dCas9 no nanostar (diffuse, no puncta). Scale bar, 5 um. B, FRAP recovery curve for KRAB-condensate Broccoli signal showing mobile fraction of 58 +/- 7% and tau = 65 +/- 8.2 s. C, Condensate number per cell: VP64 and KRAB condensate systems both show 8-12 condensates per cell; traditional systems (no nanostar) show near-zero condensates. D, FRAP mobile fraction over time (24 h to day 14) for both VP64-Condensate and KRAB-Condensate, showing modest aging (mobile fraction decreasing from ~78% to ~68% for VP64, ~72% to ~62% for KRAB). Data are mean +/- s.d. from N = 3 biological replicates.

Supplementary Tables

Supplementary Table 1 | sgRNA spacer sequences.

Designed using CHOPCHOP against hg38. All spacers target the indicated locus within 500 bp of the annotated TSS with predicted Azimuth on-target score >50.

Target Gene	Genomic Coordinate (hg38)	Strand	Spacer Sequence (5'-3')	On-Target Score
IL1B (activation)	chr2:113,587,231-113,587,250	+	GGCAGAGACACAAACTAGAC	62
ASCL1 (activation)	chr12:96,442,301-96,442,320	-	TCCGCTCGCCGCCGCCGCTC	57
TTN (activation)	chr2:179,610,422-179,610,441	+	GATCTTCTACATCTTCAGAG	54
IL1B (repression)	chr2:113,587,231-113,587,250	+	GGCAGAGACACAAACTAGAC	62
CXCL8 (repression)	chr4:74,762,101-74,762,120	-	GGAGACCTGAGAACCAAGAG	56
NFKB1 (repression)	chr4:103,527,401-103,527,420	+	GAGCAGACAGATGATGGAGA	60
GAPDH (repression)	chr12:6,537,101-6,537,120	-	TGGACAGTGAGGATGAGATG	59
HBB (repression)	chr11:5,248,001-5,248,020	+	GTGGATGAAGTTGGTGGTGA	56
MYC (multiplex)	chr8:127,740,001-127,740,020	+	GACGAGAAGGATGAGGAAGA	55
POU5F1 (OCT4) (iPSC)	chr6:31,170,801-31,170,820	-	GAGGAAGATGAGGAAGAGGA	59
SOX17 (iPSC)	chr8:55,460,001-55,460,020	+	GATGTTGTGGTGAGTGTTGA	53
Non-targeting control	N/A	N/A	GCTGAGATGATGATGATGAT	0

Supplementary Table 2 | DNA and RNA FISH probe sets.

Target	Probe Set Name	Fluorophore	Vendor
IL1B locus	IL1B-LS-Cy3	Cy3	Stellaris/LGC Biosearch
IL1B mRNA	IL1B-mRNA-CAL Fluor	CAL Fluor Red	Stellaris/LGC

Target	Probe Set Name	Fluorophore	Vendor
	Red 610	610	Biosearch
CXCL8 mRNA	CXCL8-mRNA-Quasar 670	Quasar 670	Stellaris/LGC Biosearch
NFKB1 mRNA	NFKB1-mRNA-Quasar 570	Quasar 570	Stellaris/LGC Biosearch

Supplementary Table 3 | RT-qPCR primer sequences.

Target Gene	Forward Primer (5'-3')	Reverse Primer (5'-3')	Amplicon Size (bp)	Efficiency (%)
IL1B	CCTGAGCTCGCCAGTGAAAT	GGGAACTGGGCAGACTCAAA	142	98.2
CXCL8	TTGGCAGCCTTCCTGATTTC	AAAGTGCATCAGCACTCCTC	128	97.5
NFKB1	ACAACTATGAGGTCTCTGGG	TGCCTGGATCACTTCAATTG	92	99.1
GAPDH	GTCTCCTCTGACTTCAACAGCG	ACCACCCTGTTGCTGTAGCCAA	131	96.8
HBB	GTGCATCACTGAGGCCCTGGA	CCTGGAGCTGACAGGAGTCT	118	97.3
MYC	CCTACCCTCTCAACGACAGC	TCTTGACATTCTCCTCGGTG	145	98.7
ASCL1	CAGCTGCTCAAGGCTGAGAA	GGTGAGTGGTGCTGGTGTAG	138	95.4
TTN	CAGAGCAGCAGAGAAGAGCA	TGTGGTGGTGGTGGTGGTAG	167	94.8
POU5F1 (OCT4)	CTCGAACCACATCCTCCCTC	CCTCCTGGGATGCTCTGC	122	97.6
SOX17	AGCCAGCGCAGATCAGAATC	CCTGGTGGTGGTGGTGGTAG	134	96.3
IFNB1	GAGCTACAACTTGCTTGGATTC	CAAGCCTCCCATTCAATTCCC	119	98.5
ISG15	GCGAACTCATCTTTGCCAGTA	CCAGCATCTTCACCGTCAGGT	108	97.8
IFIT1	GAAAGGCCAGAATGAGGAAG	CACCAGACTCCTCACATTTG	97	96.1
ACTB	CATGTACGTTGCTATCCA	CTCCTTAATGTCACGCAC	104	99.3

Target Gene	Forward Primer (5’-3’)	Reverse Primer (5’-3’)	Amplicon Size (bp)	Efficiency (%)
(ref)	GGC	GAT		
RPS11 (ref)	GAGAAACTGGCAAGGAGAAG	CCTCTGCATCTTCATCTTGG	176	98.6

Supplementary Table 4 | ChIP-qPCR primer sequences.

Target Locus	Forward Primer (5’-3’)	Reverse Primer (5’-3’)	Amplicon Size (bp)
IL1B promoter	CCTGAGCTCGCCAGTGAAAT	GGGAACTGGGCAGACTCAAA	142
CXCL8 promoter	TTGGCAGCCTTCCTGATTTC	AAAGTGCATCAGCACTCCTC	128
NFKB1 promoter	AGATGGCCCATGGCTTCTAT	CCTGGAGCTGACAGGAGTCT	156
IL1B TSS -5kb (control)	TAGGAGAGCAAACCCACACC	GAGACAGAAACTTGTGGTGGC	114
chr4 desert (control)	ACCCAAGTGCCTCATTCTTACC	TATATGTTGCAGAGGGCTGTCC	131
chr13 desert (control)	GGTCAGCGATTAGTGAACTTGC	CCCAAAGTCACACAGTTGTACG	118

Supplementary Table 5 | Complete nanostar RNA sequences.

[See Supplementary Note 1, Section 1.5 for complete sequences of all nanostar variants.]

Supplementary Table 6 | Plasmid list and cloning details.

Plasmid Name	Backbone	Insert	Cloning Strategy	Bacterial Strain
pAV-U6+27-Tornado-15nt-3A-Br	pAV-U6+27-Tornado-	15nt-KL A-Broccoli dsDNA	NotI/SacII ligation	DH5alpha

Plasmid Name	Backbone	Insert	Cloning Strategy	Bacterial Strain
pAV-U6+27-Tornado-15nt-3WT-Br	pAV-U6+27-Tornado-Broccoli	15nt-KL WT-Broccoli dsDNA	NotI/SacII ligation	DH5alpha
pAV-U6+27-Tornado-15nt-3A-MS2	pAV-U6+27-Tornado-Broccoli	15nt-KL A-Broccoli-MS2 dsDNA	NotI/SacII ligation	DH5alpha
pAV-U6+27-Tornado-20nt-3A-Br	pAV-U6+27-Tornado-Broccoli	20nt-KL A-Broccoli dsDNA	Gibson assembly	DH5alpha
pAV-U6+27-Tornado-15nt-3A-Pepper	pAV-U6+27-Tornado-Broccoli	15nt-KL A-Pepper dsDNA	NotI/SacII ligation	DH5alpha
pAV-U6+27-Tornado-15nt-3A-Mango	pAV-U6+27-Tornado-Broccoli	15nt-KL A-Mango dsDNA	Gibson assembly	DH5alpha
pAV-U6+27-Tornado-15nt-3B-Pepper	pAV-U6+27-Tornado-Broccoli	15nt-KL B-Pepper dsDNA	NotI/SacII ligation	DH5alpha
pAV-U6+27-Tornado-15nt-3C-Mango	pAV-U6+27-Tornado-Broccoli	15nt-KL C-Mango dsDNA	Gibson assembly	DH5alpha
pAV-U6+27-Tornado-15nt-3WT-Pepper	pAV-U6+27-Tornado-Broccoli	15nt-KL WT-Pepper dsDNA	NotI/SacII ligation	DH5alpha
pAV-U6+27-Tornado-15nt-3E-Mango	pAV-U6+27-Tornado-Broccoli	15nt-KL E-Mango dsDNA	Gibson assembly	DH5alpha
pAV-U6+27-Tornado-15nt-3F-Mango	pAV-U6+27-Tornado-Broccoli	15nt-KL F-Mango dsDNA	Gibson assembly	DH5alpha

Plasmid Name	Backbone	Insert	Cloning Strategy	Bacterial Strain
pAV-U6+27-Tornado-15nt-AB-L4-Br	pAV-U6+27-Tornado-Broccoli	15nt-KL AB-Linker-4arm-Broccoli dsDNA	Gibson assembly	DH5alpha
pCDNA3.1-dCas9-NLS	pCDNA3.1	dCas9-NLS coding sequence	NotI/XbaI ligation	DH5alpha
pCDNA3.1-VP64-MCP	pCDNA3.1	VP64-MCP coding sequence	BamHI/EcoRI ligation	DH5alpha
pCDNA3.1-KRAB-MCP	pCDNA3.1	KRAB-MCP coding sequence	BamHI/EcoRI ligation	DH5alpha
pX-dCas9-VP64	pX-dCas9	VP64 fusion	BsaI ligation	DH5alpha
pX-dCas9-VPR	pX-dCas9	VPR fusion	BsaI ligation	DH5alpha
pCDNA3.1-SAM-MS2-P65-HSF1 (GFP)	pCDNA3.1	MCP-p65-HSF1	BamHI/NotI ligation	DH5alpha
pCDNA3.1-SunTag-GCN4-sfGFP-GB1-NLS-scFv-VP64	pCDNA3.1	scFv-sfGFP-VP64 coding sequence	BamHI/EcoRI ligation	DH5alpha